Ultrasonics - Sonochemistry 56 (2019) 94–104

Contents lists available at ScienceDirect

Ultrasonics - Sonochemistry

journal homepage: www.elsevier.com/locate/ultson

Numerical investigation of design parameters for optimization of the in-situ ultrasonic fouling removal technique for pipelines

Habiba Lais[a], Premesh S. Lowe[a], Tat-Hean Gan[b,*], Luiz C. Wrobel[a]

[a] Brunel University, Kingston Lane, Uxbridge, Middlesex UB8 3PH, UK
[b] TWI, Granta Park, Great Abington, Cambridge CB21 6AL, UK

ARTICLE INFO

Keywords:
Ultrasonication
Numerical modelling
Wave propagation
Parametric study
Acoustic cavitation
Long-range defouling

ABSTRACT

Fouling build-up in engineering assets is a known problem and, as a solution, the application of power ultrasonic for in-situ fouling removal has gained much attention from the industry. Current state-of-the-art fouling removal includes the use of hydraulic, chemical and manual techniques. Much research has been conducted to advance the knowledge on the potential uses of ultrasonics across different fouling applications, primarily in reverse osmosis membranes and heat exchangers. However, the optimization of in-situ ultrasonic fouling removal has not yet been investigated and is still in its infancy. The present study uses a previously experimentally-validated numerical model to conduct a parametric study in order to optimize the technique. Focus was given to the adoption of ultrasonics for large diameter pipes. Therefore, this investigation was conducted on a 6 in. schedule 40-carbon steel pipe. Parameters investigated include: optimum number of transducers to remove fouling in long pipes from a single transducer location; performance at elevated temperature; different fluid domains; optimum voltage; variety of input signals and incremental thickness of fouling. Depending on the particular studied conditions, the possible fouling removal of up to +/−3 m from a single transducer location is demonstrated in a 6 in. schedule 40 carbon steel pipe.

1. Introduction

Accumulation of fouling is a rising problem across many industrial sectors [1], occurring on different structures such as pipelines, offshore structures and heat exchangers. The type of fouling which accumulates is dependent on the environmental conditions that surround the structure. In pipelines and heat exchangers, a common type of accumulative fouling is crystallization fouling, *i.e.* calcite formation [2]. This occurs due to the high operating temperatures causing the high temperature fluid to saturate at the walls of structures, resulting in hard-scale deposition. This crystallization fouling is extremely hard to remove and continues to accumulate from carrying the high temperature fluid, potentially leading to blockage of the pipeline. The creation of a blockage will immediately affect the efficiency of the structure and result in the operating conditions to drop below acceptable limits. The accumulation can also contribute to contamination of the fluid transported in the pipeline [3].

State-of-the-art fouling removal techniques applied in the industry include hydraulic, chemical and mechanical techniques. Each of these methods has disadvantages. For example, the use of hazardous chemicals has negative impact on the environment and purity of fluid, leading to production/operation halts for maintenance and, very critically, often posing danger to workers who carry out the procedures [4].

Another popular method of fouling removal is the use of ultrasound. Currently, ultrasonic baths are used for cleaning individual components submerged in a bath where cavitation bubbles are generated within the fluid, implode at the surface of the fouling. Research into the use of ultrasonic baths for fouling removal has been carried out for Reverse Osmosis applications [5–7]. This method demonstrates successful fouling removal but requires halting the production/operation to submerge the components in the ultrasonic bath, and crucially is restricted to small sized components. This paper investigates the use of ultrasonic power for in-situ fouling removal and uses a previously experimentally validated finite element model to optimize the process [8].

The layout of the paper is as follows. The ultrasonic fouling removal methodology and state-of-the-art is discussed in Section 2 while Section 3 presents the numerical study. Section 4 contains numerical results and analysis which are further discussed in Section 5 with concluding remarks.

* Corresponding author.
E-mail addresses: tat-hean.gan@brunel.ac.uk, bic@brunel.ac.uk (T.-H. Gan).

https://doi.org/10.1016/j.ultsonch.2019.03.027
Received 7 June 2018; Received in revised form 26 March 2019; Accepted 27 March 2019
Available online 03 April 2019

2. State-of-the-art

2.1. Theoretical background

The fouling removal mechanism with High Powered Ultrasonic Transducers (HPUT) is by the generation of acoustic cavitation. This is the formation of vapour/gas bubbles which result from sudden decreases in the pressure in a liquid caused by a compressional vibration [9]. A rarefaction instant is introduced during a decrease in wave pressure which forms a vacuum where a bubble can form. During the oscillation of the bubble, the radius of the bubble increases in the rarefaction instants and decreases during the compressional instants. In one of these cycles, the compression can burst the bubble to produce a pressure of up to 500 Bar and a temperature of up to 5000 °C. In recent studies, it has been found that cavitation bubbles do not nucleate homogenously and instead, heterogeneously from a gas cavity or from existing stabilized micro-bubbles within the liquid [10].

There are two types of cavitation bubbles that can form within a liquid. The first is stable cavitation where bubbles oscillate for long period of time over a number of cycles before its implosion. Transient cavitation lasts for less than one cycle and is violent enough to potentially damage any surface in contact with the liquid [11]. Each type of cavitation results in different fouling removal mechanisms such as microstreaming, shear forces and high temperatures. For the present application, transient cavitation is required to generate shear forces and shock waves to dislodge fouling on the surface of the structure. Fig. 1 illustrates two types of cavitation bubbles that can be generated with resulting fouling removal mechanisms. Although cavitation is a known phenomenon that can damage a structure by the strong forces created in the violent implosions [12], literature has demonstrated the development and implosion of cavitation bubbles to be the primary fouling removal mechanism in ultrasonic fouling removal [13]. Experimental research supports the notion that these implosions do not damage the structure during fouling removal. An example of this is Reverse Osmosis Membrane studies [12].

2.2. Ultrasonic fouling removal technique

Prior work has discussed conventional ultrasonic defouling and the disadvantage of needing to halt operations of the facility for cleaning to commence [8,14]. The technique proposed in this paper is a non-invasive fouling removal solution using ultrasonic waves [15,16] to vibrate a structure and generate cavitation bubbles within the fluid contacting the fouled surfaces. This solution places an array of bespoke HPUTs on the outer wall of the pipe structure which is filled with a cavitating liquid (typically water). Fig. 2 shows the modification of the

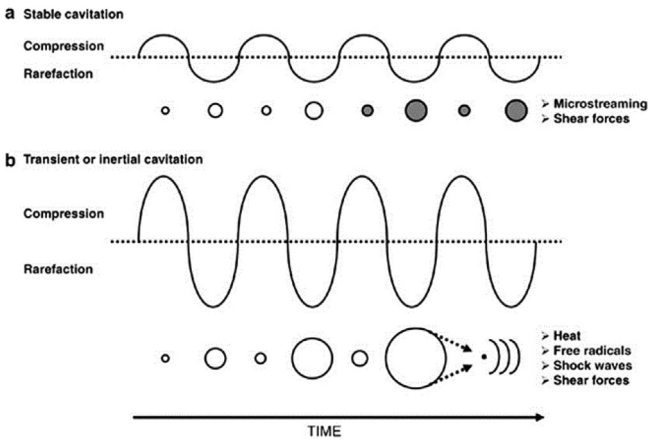

Fig. 1. Illustration of cavitation bubbles displaying stable and transient cavitation.

Fig. 2. HPUT before modification (left) and after machined curvature on HPUT contact surface (right).

HPUT for attachment to curved structures with maximum surface contact.

The HPUTs are assembled by bolting the front and back masses to sandwich stacked piezoelectric ceramic rings. The materials of these components are dependent on the mechanical and chemical properties desired with the HPUT excitation. There are various parametric considerations when configuring an array of transducers for successful cleaning, which have been identified as:

- Transducer attachment method.
- Bespoke transducers for ultrasonic defouling applications.
- Acoustic impedance mismatch between the structure and the HPUT.
- Power amplifier and input signal generation (power level, frequency, waveform, etc.).

The transducer is excited at its resonant frequency to generate cavitation bubbles within the liquid. The resonance of the HPUT is dependent on the modifications carried out on the selected transducer, which shifts the resonant frequency and also affects the impedance. The implosion of bubbles on the surface of the fouling layer results in removal of fouling but the vibration of the structure itself also contributes to the removal of fouling.

2.3. Optimization of ultrasonics

Research into improving the ultrasonic fouling removal technique has focused on optimizing the cleaning parameters such as cleaning time, frequency and cleaning agent. Different methods have been used to investigate the parameters describing optimization of cleaning, transducers and applications for the specific problem. These include experimental testing and modelling.

2.3.1. Experimental

Examples of research for improving the ultrasonic technique include boat cleaning [17] and the system uses ultrasonic as a preventative method of fouling. The efficiency of the transducers has been determined through testing on contaminated samples experimentally, which is a costly and time-consuming approach to determining the effectiveness of the selected ultrasonic device and its parameters. The effectiveness of ultrasonic defouling based on pH level, ionic strength and particle size has also been studied [18]. The study found various empirical trends such as both low and high pH solutions being more effective compared to neutral solutions. The effects of frequency (28, 45 and 100 kHz) on ultrafiltration and membrane cleaning [19] concluded that 28 kHz was the most effective whereas 100 kHz had little effect. The use of low frequencies to enhance permeating flux was studied and found that low power enabled at these frequencies can minimize damage to the membrane surface [20].

Nguyen et al. [21] focused on a green technology for cleaning

turbine engine oil filters on ships with ultrasonics. The study used a 25 kHz multi-transducer system. Under experimental conditions, various parameters were explored including power (300 W and 600 W), temperature effect, ultrasonic defouling times, and pressure losses through oil filters and solvent for washing. The cleaning efficiency was compared for three cases; hand washing, preliminary washing and ultrasonic washing. The experimental data were correlated using a statistical analysis method and it was concluded that ultrasonic washing was the most effective and time efficient.

Experimental work has been carried out to ultrasonically remove contaminants on plastic parts [22]. The study investigated different cleaning agents and temperature, and also suggested an optimal operation time and frequency for cleaning. After selecting the optimal parameters, a field trial was implemented to demonstrate the practical effectiveness and time-efficiency of the method. Further work has been carried out on optimising the ultrasonic defouling technique for membrane fouling removal using time-domain reflectometry (TDR) [23]. TDR was shown capable of detecting membrane fouling in real time and also detected the removal of the fouling during ultrasonication. This method can optimise the cleaning runtime.

Generally, experimental investigation of optimisation of the ultrasonic fouling removal technique is very time-consuming and costly. Very few parameters can be investigated as it can be hard to obtain transducers of various frequencies and power. Also, creating an experiment that can control different structural variables such as fluid temperature, fouling thickness can also be difficult to achieve.

2.3.2. Numerical simulation

In contrast to experimental parameter studies, numerical simulations allow studies with lower cost and time implications.

Finite Element Analysis has been used in 2D conditions to calculate the sound field distribution within a water tank to optimize the parameters governing effective cleaning [24]. FEA has also been used to design and test the flow through a separator [25]. Three models were investigated, separation model (particle fluid mixture), flow model (CFD flow profile) and transducer model (electroacoustic model of the cell). Overall, the models contributed towards fine tuning the performance of the cell.

Another approach that has been investigated combines numerical simulation and automated optimization differentiation to design ultrasonic Langevin transducers [26]. This work focused only on the modelling aspects without any experimentation to prove the method works for designing ultrasonic horn attachments.

An in-depth review has been carried out on modelling the acoustic pressure within a sonochemical reactor [27]. Various models have been discussed, including linear and non-linear modelling, of the two, non-linear modelling was able to account for the attenuation caused by cavitation bubbles within the sonochemical reactor. The ultrasonic transducer has also been discussed. This is a relatively easy model to create using electromechanical physics. Overall, numerical simulations of sonochemical reactors can model the vibration of the walls and the acoustic pressure field. The effect of cavitation on wave propagation is significant and can only be taken into account within a nonlinear model. Some work has been done to model the generation of cavitation bubbles.

Numerical modelling has also been used to improve the ultrasonic fouling removal technique by correlating the high intensity sound field with the generation of cavitation [28]. The modelling investigates the wave propagation into a cavitating liquid model (two-phase continuum). The results show qualitative agreement with the pressure antinodes and locations of cavitation generation in the experimental validation. In recent work, the use of multiple transducers at moderate power levels has shown to be more effective than using a single transducer at higher power levels [29], which promises improvement of the ultrasonic defouling coverage using a transducer array. The use of FEA for advancing the design and upscaling of the ultrasonic defouling technique for reactors is promising, and it was been reported by Jordens et al. [29].

Effective extensions of linear acoustics have been proposed in Caflish et al. [30]. The effective equations have been applied [31] where they are most suitable for low amplitude waves or weakly non-linear conditions [27]. Similar methods have been applied for reasonable amplitude waves [32,33] but their use is restricted for inertial cavitation due to the amplitude of waves ranging below the Blake threshold. Some attempts have been made to extend the Caflisch model with the purpose of simulating larger wave amplitudes; however, this is limited to small spatial regions [34].

In recent years, COMSOL Multiphysics' capabilities in coupling a variety of physics phenomena has made it popular for modelling sonochemical reactors and for optimizing design parameters. Cavitation activity generated by ultrasonic horns has been investigated using COMSOL [35,36]. The optimization of reactor dimensions has also been carried out in COMSOL to couple the vibration of the walls and the sonochemical activity within the fluid domain [37,38]. Several variables have been considered for reactor optimization, including frequency and ultrasonic intensity, however, the reactor geometry has the most significant effect [37–40].

COMSOL has also been used to generate a model based on the Caflisch model, producing reasonably good estimates of the acoustic pressure field and the approximate cavitation zones [41,42–44]; however, although this work includes a rigorous approach, the tests have some unjustified simplifying assumptions.

From the various linear and non-linear modelling methods, the prediction of cavitation is a phenomenon which is not close to being solved numerically. However, FEA does provide insight into the potential wave propagation and can assist as a useful design tool but this cannot completely avoid experimental investigation and validation.

3. FEA theory and methodology

3.1. FEA validation

An experimental set-up was constructed to first prove that the ultrasonic fouling removal technique can in fact remove fouling from the inner walls of a pipe sample. This experimental work was presented in the thesis of de Carellan [45]. Having produced a sample with successful cleaning patterns, COMSOL Multiphysics 5.2a was used by the present authors to create a model of the experimental configuration to match the cleaning results, specifically the pressure distribution and solid displacement [8,14]. A reasonable correlation was achieved on the FEA results compared to the experiments conducted using the 3D Laser Scanning Vibrometer.

3.2. Layout of the FEA model

Once the COMSOL model was validated with successful cleaning results achieved in previous experiments, this numerical methodology is applied to a 6 in. schedule 40 API 5L/A106 carbon steel seamless tube with 168 mm outer diameter, 7.11 mm wall thickness and 6 m length. The present paper conducts a parametric study to investigate the optimal HPUT array (see Fig. 3) with water filled within the pipe (static), fouling, signal input and fluid temperature. The model focuses on a 40 kHz Langevin bolt-clamped HPUT due to its successful cleaning in prior experiments [8,14,46]. The pipe is monitored at different locations along its length to compare the various parameters as shown in Fig. 4. The points are placed at 1 m distances on the inner and outer walls of the pipe to monitor the acoustic pressure within the liquid and the solid displacement on the outer wall of the pipe.

The geometry is designed assuming symmetry to reduce the computational time of the model as shown in Figs. 5 and 6. The number of planes of symmetry is dependent on the number of transducers under investigation. Physics are assigned within the model to account for the

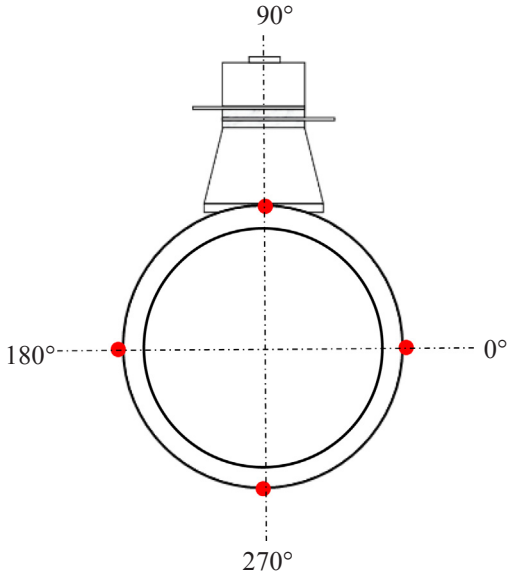

Fig. 3. Illustration of HPUT configurations for FEA analysis.

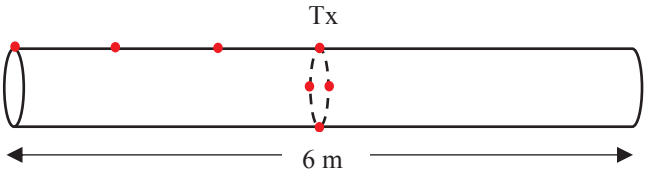

Fig. 4. Schematic of excitation of schedule 40 pipe and monitored points.

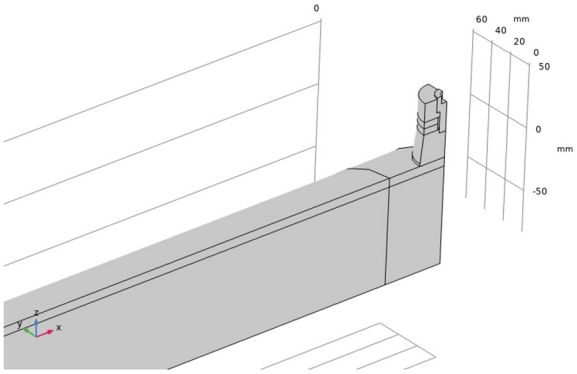

Fig. 5. Geometry of 4-Transducer configuration on a 6 m, 6 in., schedule 40 carbon steel pipe.

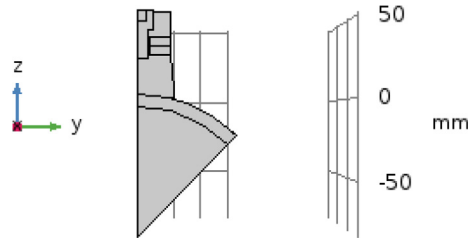

Fig. 6. Cross sectional view of geometry of 4-Transducer configuration on a 6 m, 6 in., schedule 40 carbon steel pipe.

transducer, solid pipe and fluid domain within the pipe. The fluid surrounding the outer pipe is considered to be atmospheric air, which is not modelled in this work; instead the walls in contact with the air are assumed as 'free'.

- Pressure Acoustics, Transient – fluid domain
- Electrostatics – piezoelectric ceramic components of the transducer
- Solid Mechanics – elastic components of the transducer and pipe
- Piezoelectric Effect – coupling of the piezoelectric components with elastic components
- Acoustic-Structure Boundary – coupling of the interface between the inner pipe wall and fluid domain

The Pressure Acoustics model uses the wave equation:

$$\frac{1}{c^2}\frac{\partial^2 p}{\partial t^2} + \nabla^2 p = 0 \tag{1}$$

where, p is the acoustic pressure and c is the speed of sound in the liquid, which is assumed constant.

The linear elastic behavior is used for the solid parts of the model. All solid parts excluding the piezoelectric ceramic rings will obey their material properties and are considered to be of linear elastic material. The application of Newton's law yields the following equation:

$$\rho_S \frac{\partial^2 \boldsymbol{u}}{\partial t^2} = \nabla \cdot \bar{\bar{\mathbf{T}}} \tag{2}$$

where, $\boldsymbol{u}$ is the solid displacement field, $\bar{\bar{\mathbf{T}}}$ is the stress tensor, and ρ_S is the density of the solid.

Piezoelectric material is assigned to the piezoelectric ceramic rings which obey the solid mechanics governing equations and, additionally, the PZT-linearized constitutive equations in stress-charge form:

$$\bar{\bar{\mathbf{T}}} = c_E \cdot \bar{\bar{S}} - e^t \cdot \boldsymbol{E} \tag{3}$$

$$\boldsymbol{D} = e \cdot \bar{\bar{S}} + \varepsilon_S \cdot \boldsymbol{E} \tag{4}$$

where, $\bar{\bar{\boldsymbol{T}}}$ is the stress tensor, $\bar{\bar{S}}$ is the strain tensor, $\boldsymbol{E}$ is the electric field, $\boldsymbol{D}$ is the electric displacement field, c_E is the elasticity matrix, e is the piezoelectric coupling coefficient for the stress-charge form, ε_S is the permittivity matrix.

Electrostatic phenomena is assigned to the piezoelectric ceramic rings where the signal is applied using the following formula:

$$\nabla \cdot \boldsymbol{D} = 0 \tag{5}$$

$$\boldsymbol{E} = -\nabla V \tag{6}$$

where, V is the electric potential corresponding to the electric field $\boldsymbol{E}$.

The piezoelectric ceramic rings are made of PZT-4 and their material properties are selected from the built-in database in COMSOL. The terminal and ground equipotential are applied to the boundaries explicitly as in previous work [8]. The ground boundary is set equal to 0 V and the terminal boundary is set to:

$$V = V_0 \tag{7}$$

where, Vo is the modulated input signal. The correct polarization is achieved by assigning a rotated global co-ordinate system to one of the two piezoelectric ceramic rings to rotate its polarization downwards.

Multiphysics modules are assigned to couple the pressure acoustics and solid mechanics physics across the acoustic-structure boundary between the fluid and solid domains. This allows the radiation of the wall due to transducer excitation to be taken into account and creates high and low pressures to propagate into the fluid domain [47]. For this reason, COMSOL is used to incorporate the required physics to simulate the experimental configuration for the present study.

The COMSOL model mimics the transducer attachment by using integration on the boundary between the transducer contact surface and pipe surface. This model ignores the transducer holder and instead, a fixed constraint is placed on the top of the transducer bolt to represent the fixed contact between the transducer holder and the transducer itself. As this model neglects the presence of cavitation bubbles, the resulting attenuation and acoustic radiation effects are not considered [48]. However, attenuation has been achieved by altering the bulk viscosity of the fluid domain.

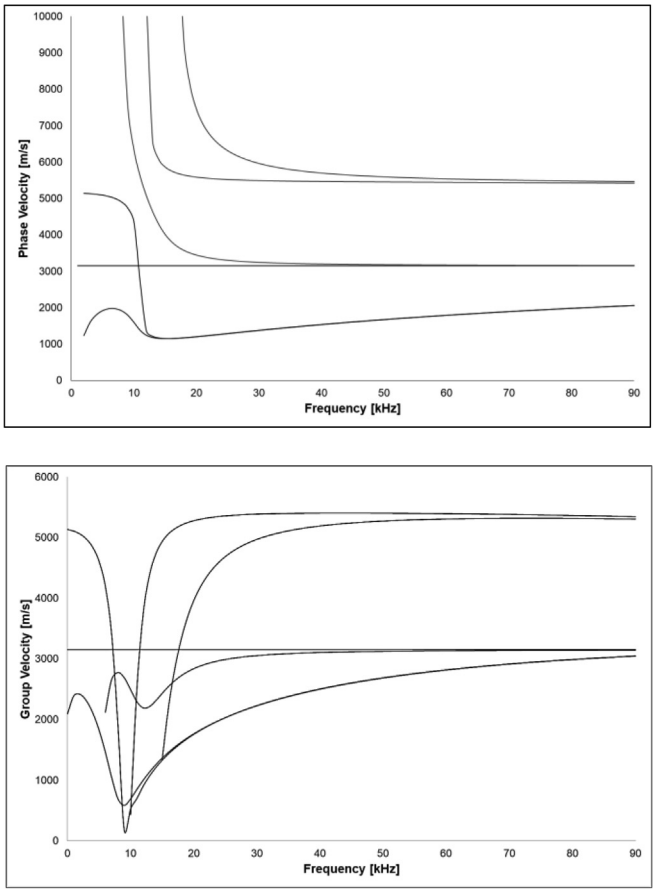

Fig. 7. Dispersion curve for 6 in. schedule 40 carbon steel pipe cross section [49].

A dynamic transient simulation to map out the wave propagation requires the calculated mesh to be optimal. The wave equation requires the time stepping within the solver to complement the meshing itself to yield an accurate solution. The meshing size uses ten 2nd-order elements per wavelength. The equation used to calculate the maximum allowed mesh element size (*ho*) is given by:

$$h_o = \frac{c}{Nf_o} \tag{8}$$

where, c is the group velocity, N is number of elements per wavelength and f_o is the center frequency.

The dispersion curves for the 6 in. diameter schedule 40 carbon steel pipe is shown in Fig. 7 [49]. The dispersion curve graph illustrates the wave velocity in relation to the frequency which separate curves for each of the existing wave modes in a frequency region. Fig. 7 shows the fundamental axisymmetric wave modes (longitudinal and torsional) as well as the corresponding first flexural wave modes produced over frequency range.

In typical pipeline sizes and test frequencies (20–100 kHz) the three axisymmetric guided wave modes that can be excited as L(0,1), L(0,2) and T(0,1) [15]. Longitudinal axisymmetric wave modes are denoted by L(0,m) and torsional axisymmetric wave modes are denoted by T(0,m). Non-axisymmetric flexural wave modes are denoted by F(n,m). This nomenclature was suggested by Meitzler [50] and popularized by Silk and Bainton [51]. According to this nomenclature, vibration modes in cylindrical structures are based on the following format:

$$X(n, m) \tag{9}$$

where, x represents the character to denote whether the vibration modes are longitudinal and axisymmetric (L), torsional and axisymmetric (T) or non-axisymmetric (flexural) (F). The n is a positive integer giving the identification of harmonic vibrations of displacement around the circumference and m, is a positive integer to indicate the incremental order of the modes of vibration within the wall. At lower frequencies (< 30 kHz) the wave modes are more dispersive compared to high frequencies where the group velocity reaches a constant value. The group velocity is selected using the dispersion graph in Fig. 7 for this numerical study. *Free Tetrahedral* elements are used for a high density around the transducer location, the remainder of the geometry is swept as followed:

$$Sweep\ density = \frac{2800\,mm}{h_o} \tag{10}$$

The selected study for this model is *Transient*, so that the simulation can generate results as the modulated wave propagates from the transducer.

The increments are based on the maximum allowed mesh element size. The time steps are chosen to resolve the wave equally over time whilst the meshing is placed to resolve the wave propagation over the model itself. Time steps must be optimized relative to the mesh and this is supported with the relationship between mesh size h_o and observation time step (Δt):

$$t_x = \frac{c\Delta t}{h_o} \tag{11}$$

The t_x ratio is given as 0.2 as it is suggested to be near optimal [52] and by rearranging Eq. (11), the time steps are calculated using (12):

$$\Delta t = \frac{t_x h_o}{c} = \frac{0.2 h_o}{c} \tag{12}$$

The simulation duration is selected based on the Time of Arrival which is calculated using the group velocity of the longitudinal mode found for the 6 in. schedule 40 API 5L/A106 carbon steel seamless tube with 168 mm outer diameter, 7.11 mm wall thickness (see Fig. 7). The Time of Arrival can be calculated as follows:

$$Time\ of\ Arrival = \frac{x}{c_l} \tag{13}$$

where x is the distance between the transducer location and end of pipe and c_l is the group velocity of the longitudinal wave mode at the excitation frequency.

To ensure that standing waves are achieved, the time of arrival must be calculated based on the signal arriving at the end of the pipe and travelling back to the excitation location, totaling 6 m in travelling distance. Extra time must also be taken into account to accommodate multi-modal responses (higher order flexural modes); therefore, the time duration has been selected for a total of 15 m of distance.

3.3. Transducer array

The number of HPUTs within a configuration is investigated, as a single transducer may not develop high enough values of pressure within the fluid to generate cavitation, depending on the diameter of the pipe, wall thickness and pipe length. For the pipe sample of interest, the diameter allows multiple transducers to be placed around the circumference to potentially increase the acoustic pressure within the fluid and the outer wall displacement. The numbers of transducers being investigated are 1 (90°), 2 (90° and 270°) and 4 (0°, 90°, 180° and 270°).

The configuration is placed at the mid-length of the 6 m pipe. Symmetry is applied to each configuration to reduce computation time.

The selected optimal transducer array for long-range cleaning is utilized for further investigation of the following removal parameters:

- temperature of fluid (20 °C, 50 °C and 100 °C)
- input signal (sinusoidal and square)
- layer of fouling (calcite)

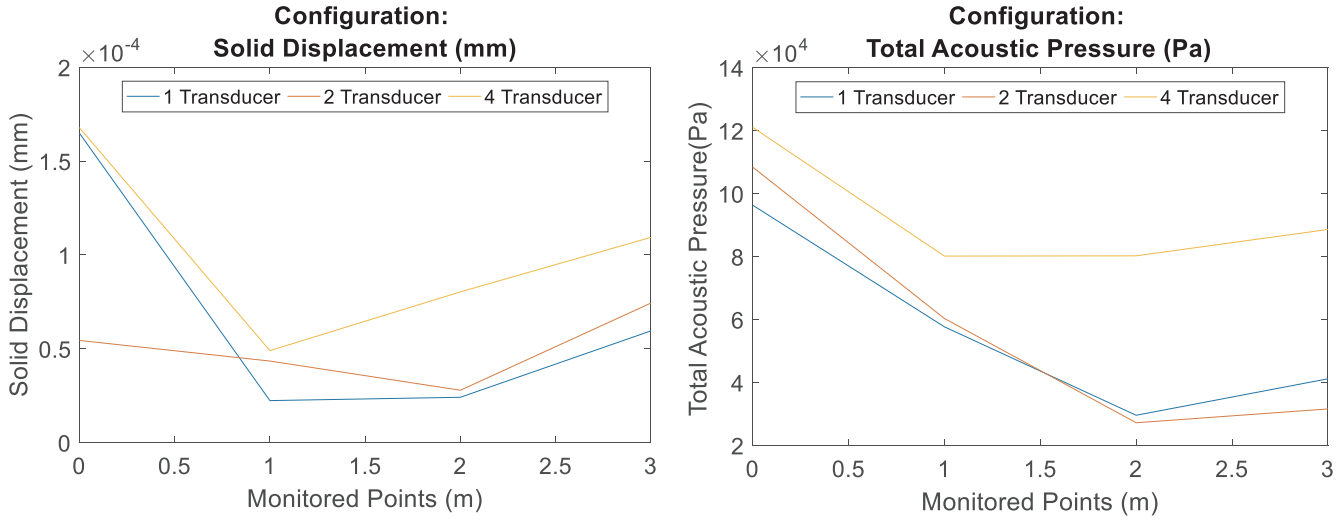

Fig. 8. Maximum solid displacement and pressure acoustic at monitored points for each investigated transducer configuration.

- Number of cycles (10 and 20)

The data obtained will primarily focus on the pressure acoustics and solid displacement at the monitored points.

4. Results and analysis

The results of the FEA parametric study were compiled to compare the solid displacement and acoustic pressure at monitored points along the length of the pipe (0, 1, 2, 3 m).

To compare the coverage and amplitude achieved from each configuration, the maximum amplitude of solid displacement and acoustic pressure is measured from the monitored points along the length of the pipe. Polar plots are created for each configuration at the maximum amplitude at different locations to analyze the coverage over the cross-section of the pipe wall.

Comparing the amplitude at the monitored points for the different configurations in Fig. 8, the trend shows that the 1-Transducer achieves its maximum displacement and acoustic pressure amplitude at the transducer location; along the length of the pipe, the 1-Transducer case reduces in amplitude, resulting in an average acoustic pressure of 3 KPa.

Comparing each configuration at the excitation location, the 2-Transducer case achieved the lowest displacement, due to the configuration resulting in superposition of the signals. The remainder of the 2-Transducer results follows a similar trend to the displacement amplitude achieved for the 1-Transducer case.

For the acoustic pressure, with the increase of transducers, the achieved amplitude at the transducer location also increases. For the remainder of the pipe length, the 1-Transducer and 2-Transducer case follow a similar trend with an average of 3 KPa.

The 4-Transducer case has shown to achieve the highest displacement and acoustic pressure at each monitored point, averaging 8 KPa for the remainder of the pipe length.

The polar plots in Fig. 9 for the 1-Transducer case show high amplitude at the transducer location for both the displacement and acoustic pressure. For the remainder of the circumference, the displacement averages below 0.5×10^{-4} mm. the acoustic pressure shows some peaks reaching 4 KPa at 0° and 180°. The remainder of the circumference has an average of 2 KPa of pressure being achieved. This coverage is not ideal for long distance due to the drop in amplitude and the lack of uniform coverage being achieved.

The 2-Transducer case achieves its highest amplitude at the transducer locations (90° and 270°) as shown in Fig. 10. Over the length of the pipe, the amplitude of these peaks drop. The remainder of the circumference averages below 0.5×10^{-4} mm and 5 KPa. At 0° and 180°, the peak achieved in the acoustic pressure shows a blunt feature, this could be due to superposition related to the transducer spacing.

The highest amplitude for the displacement and acoustical pressure is achieved in the 4-Transducer configuration at 0°, 90°, 180° and 270° as shown in Fig. 11. The configuration achieved a more uniform coverage as well as higher averaging coverage for the displacement (1×10^{-4} mm) doubling the average shown in the 1-Transducer and 2-Transducer cases. The acoustic pressure averages approximately 7 KPa.

The study of the HPUT array has shown that the transducer location should typically achieve the same displacement due to the vibration of the transducer but the 2-Transducer case has a reduction as mentioned previously due to superposition. The increase in the number of transducers improves the coverage achieved at the transducer location and has increased the acoustic pressure within the fluid domain. The 4-Transducer case has also shown to achieve high amplitudes at further distances compared to the 1-Transducer and 2-Transducer cases showing its promise for achieving long distance cleaning coverage.

The 4-Transducer configuration was selected for further parametric analysis of the cycle input, fluid temperature, addition of fouling and signal input.

The number of cycles of the sinusoidal input signal is investigated and displayed in Fig. 12. For the displacement, the increase in cycles has in increase in the displacement being achieved on the outer wall of the pipe; however, for the acoustic pressure, this does not have an effect. This implies that the number of cycles does not improve the delivery of the signal through the pipe wall thickness, into the fluid domain.

The effects of temperature of the fluid domain is investigated and displayed in Fig. 13. At the transducer location, the displacement increases at 50 °C whereas the 20 °C and 100 °C remain the same. Along the length of the pipe, the displacement amplitude increases for 50 °C and 100 °C compared to 20 °C. This suggests that the increase in temperature improved the propagation of the vibration from the transducer for longer distances.

The 50 °C case increases the acoustic pressure of 3 Bar at the transducer location whereas the 100 °C achieves 2 Bar, this could be due to the temperature being at the boiling point of water, the fluid used in this model. This can suggest that the increase of temperature can increase the acoustic pressure however, when reaching boiling temperature, this will decrease. Overall, acoustic pressure achieved along the length of the pipe does not fluctuate compared to the 20 °C case.

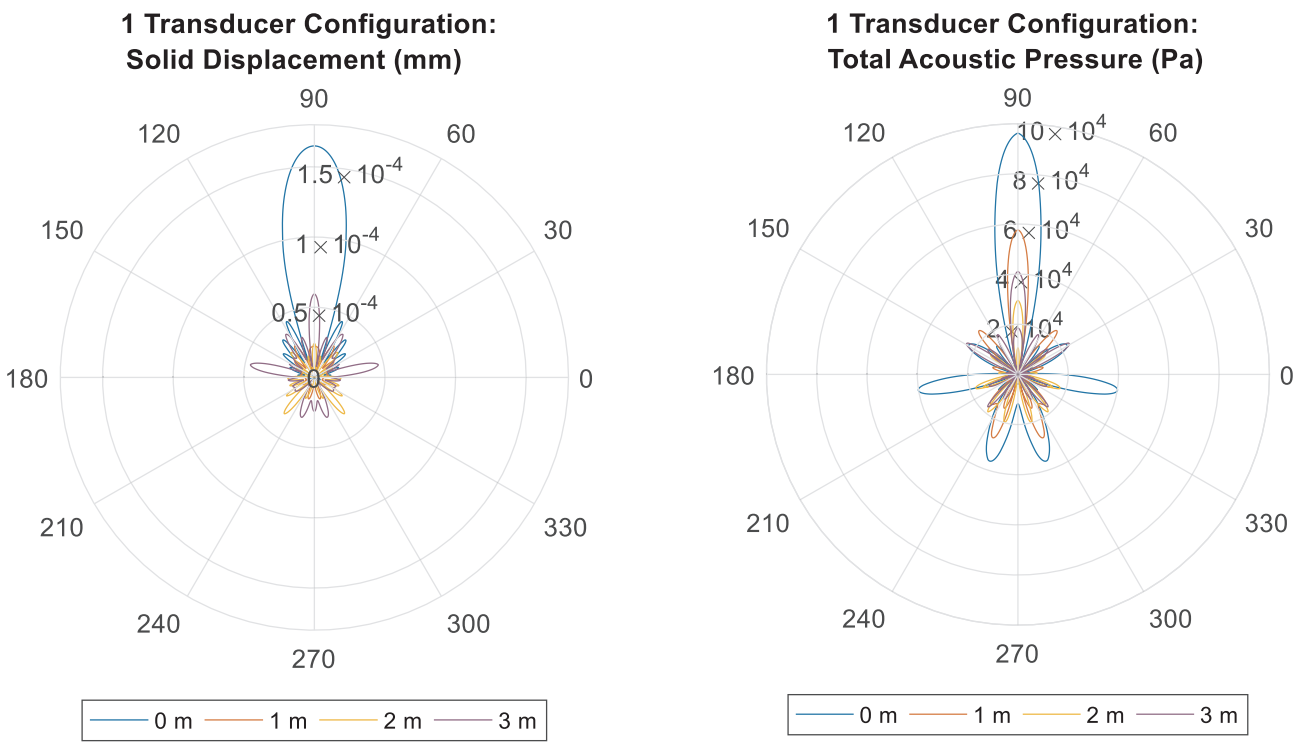

Fig. 9. Solid displacement and acoustic pressure polar plots for 1 HPUT case, displaying the maximum amplitude at each monitored point.

The addition of a 3 mm thick calcite layer on the inner wall of the pipe is then investigated (see Fig. 14). The displacement shows to have a small variation at the excitation location however, along the length of the pipe, the amplitude fluctuates between high and low amplitudes. This could suggest that the addition of the calcite has affected the wave propagation across the structure, resulting in a shift in the nodes and antinodes at the monitored points.

The acoustic pressure shows a reduction due to the addition of calcite at the transducer location, which could be explained by the calcite layer attenuating the vibration through the pipe thickness into the liquid domain. At 1 m, there is an increase in acoustic pressure which matches to the high displacement. The remainder of the acoustic pressure of the calcite matches similarly to the increase and decrease in displacement. This shows that the calcite layer attenuates the wave

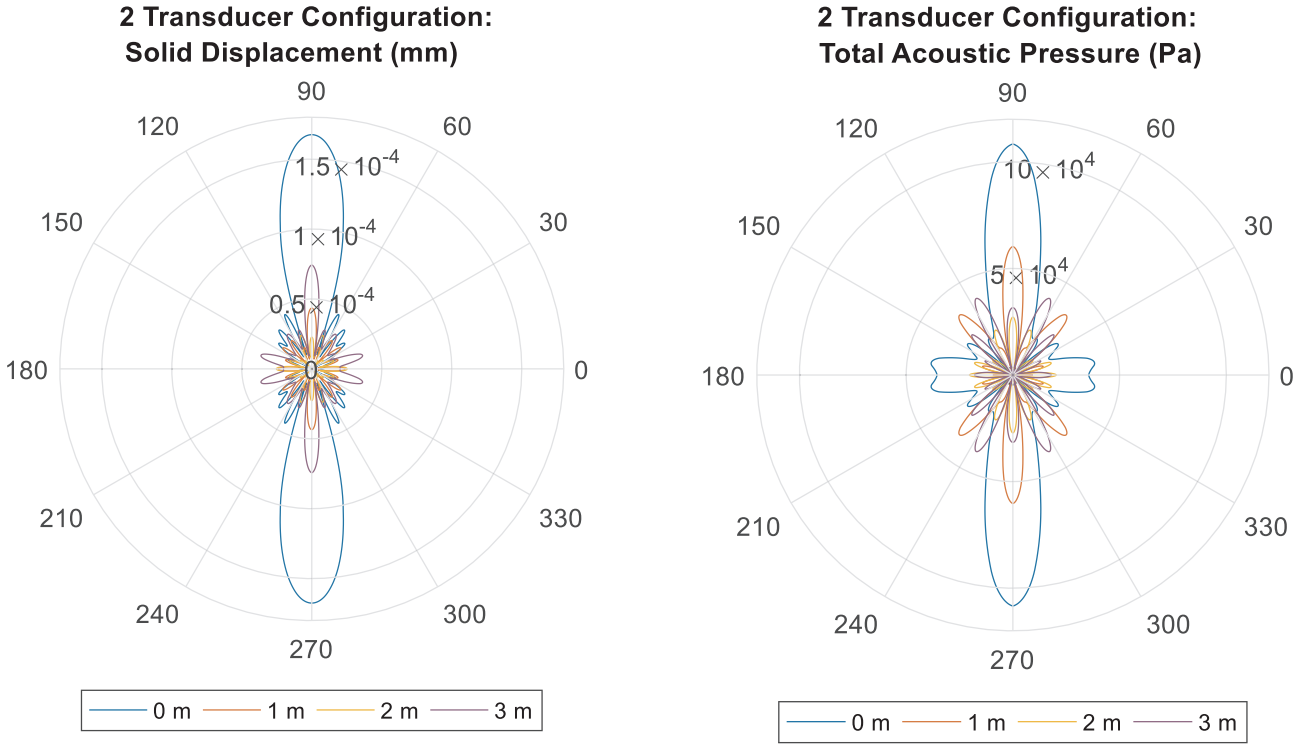

Fig. 10. Solid displacement and acoustic pressure polar plots for 2 HPUT case, displaying the maximum amplitude at each monitored point.

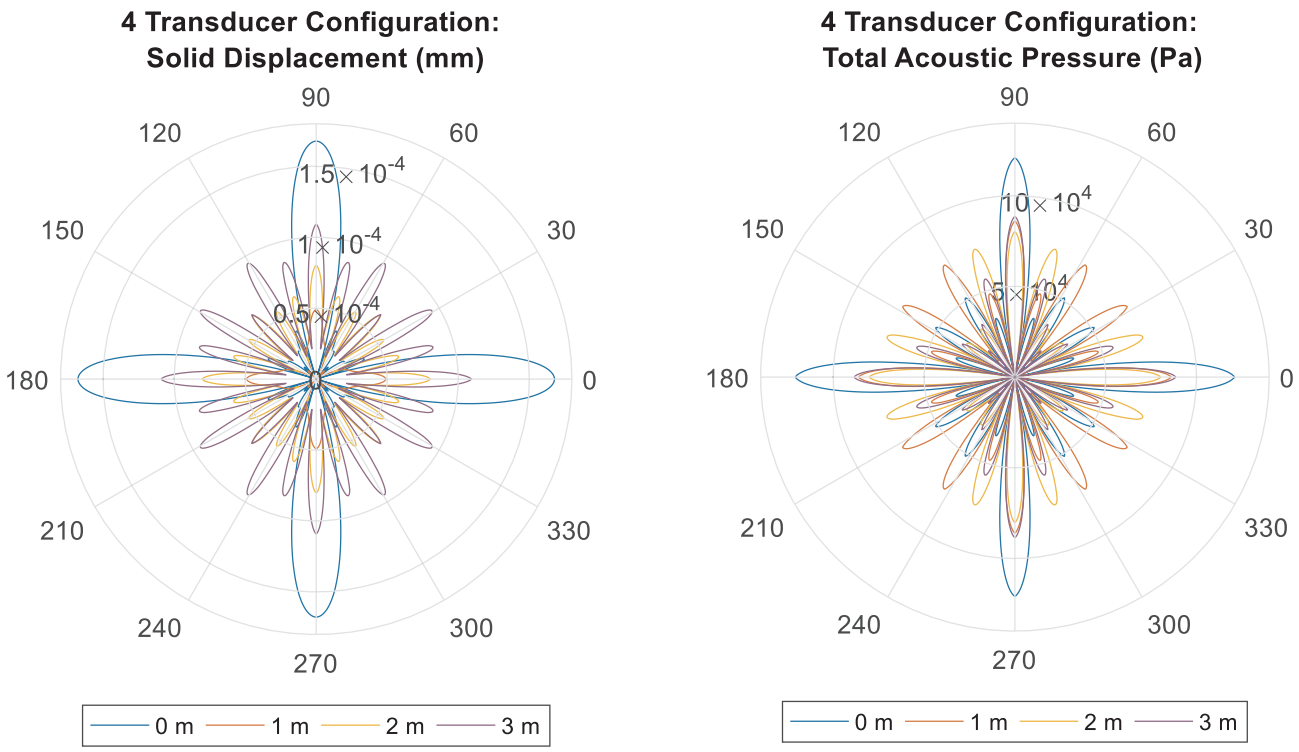

Fig. 11. Solid displacement and acoustic pressure polar plots for 4 HPUT case, displaying the maximum amplitude at each monitored point.

propagation and this was experimentally studied by the present authors in 2018 [49].

When investigating an alternative waveform to the sinusoidal input in Fig. 15, it is shown that the square wave input has increased the displacement and the acoustic pressure across all monitored points. The acoustic pressure achieves the minimum 1–2 Bar of pressure which is the known threshold to generate cavitation for a 40 kHz transducer [53]. This provides more evidence that the 4-Transducer case can potentially achieve long-range cleaning by creating pressure amplitudes above the cavitation threshold.

Fig. 16 shows the displacement on the outer wall of the pipe when exciting the 4-Transducer configuration. The outer wall achieves a uniform displacement propagating from the transducer location.

5. Discussions and conclusions

This work uses a non-invasive method of fouling removal using power ultrasonics. The technique itself is carried out by using tailored bespoke HPUTs attached directly to the outer wall of the structure (inner wall of pipe is filled with liquid). The excitation of the HPUT occurs at its natural resonant frequency and results in cavitation bubbles within the liquid. The implosion of these bubbles occurs in regions of high pressure, favorably on the fouled surface results in forces large enough to remove the fouling.

FEA methodology has been validated in previous work by the present authors [8,14] and was used in this study to investigate the effects of different parameters and to optimize the transducer configuration and input variables for cleaning a 6 m long 6 in. schedule 40 carbon steel pipe.

The 1-Transducer case showed itself suitable only for localized

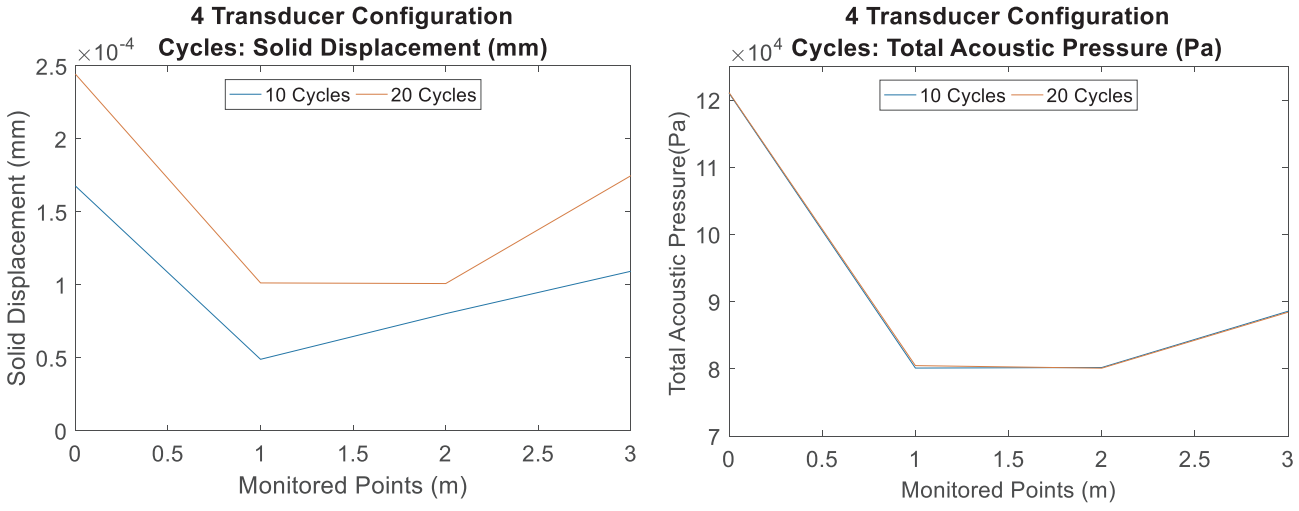

Fig. 12. Maximum solid displacement and pressure acoustic at monitored points for each investigated number of cycles.

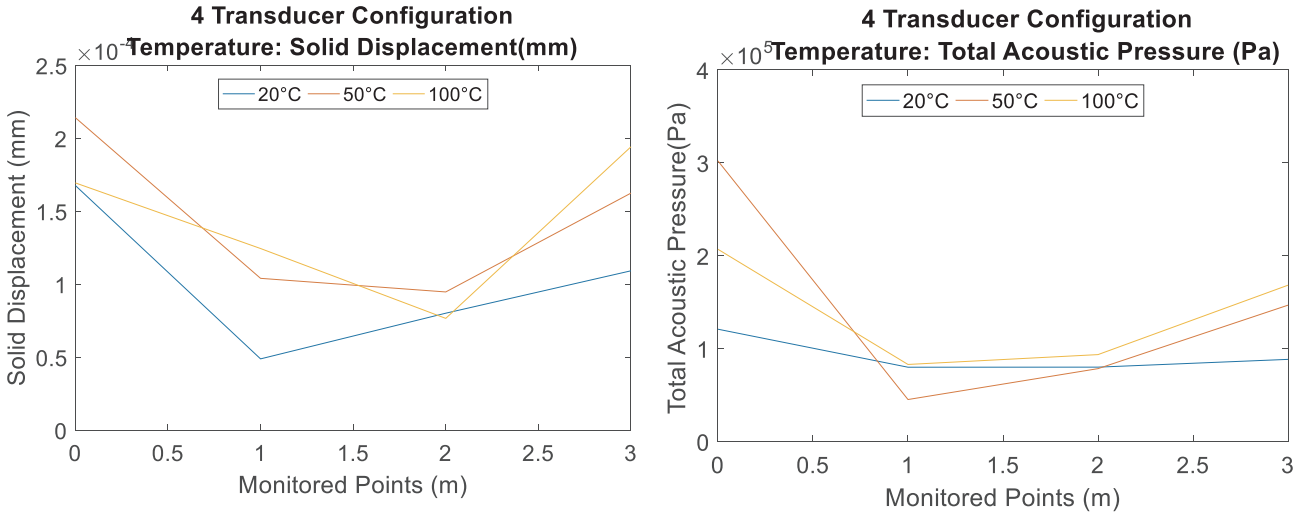

Fig. 13. Maximum solid displacement and pressure acoustic at monitored points for each investigated fluid temperature.

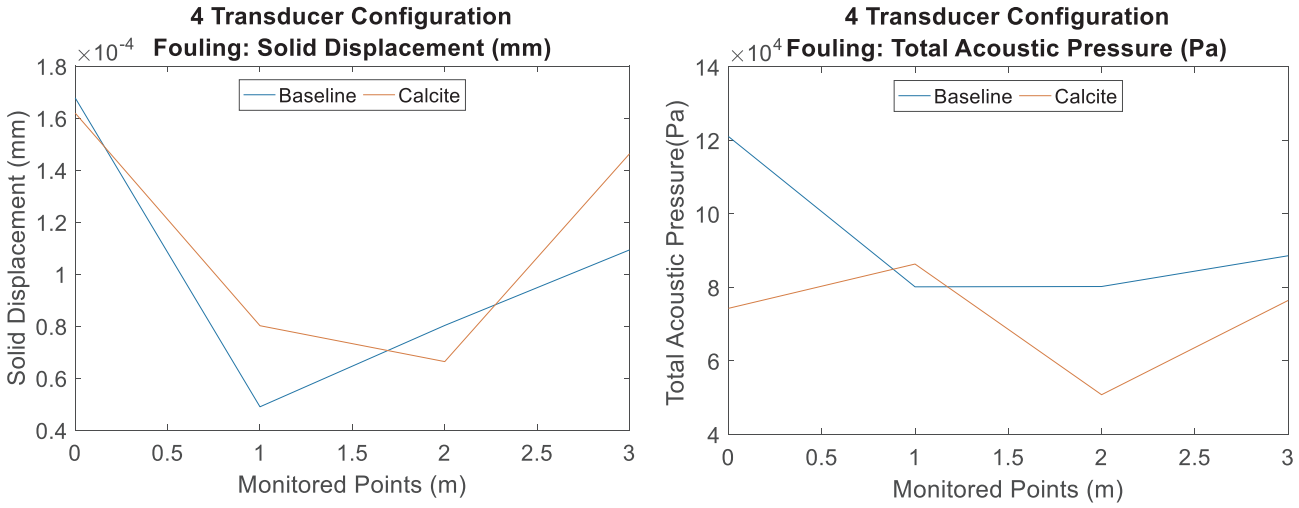

Fig. 14. Maximum solid displacement and pressure acoustic at monitored points for each investigated non fouling and fouling case.

fouling removal as it does not propagate far, and can be used for specific applications such as fouling removal in pipe elbows or bends.

The study showed that the 4-Transducer case was the most suitable for long range fouling removal for the studied conditions as it had achieved high pressure and displacement along the length of the pipe. This configuration also achieved a uniform distribution at the circumference at different locations along the length of the pipe.

The parametric study also showed the square waveform input has an

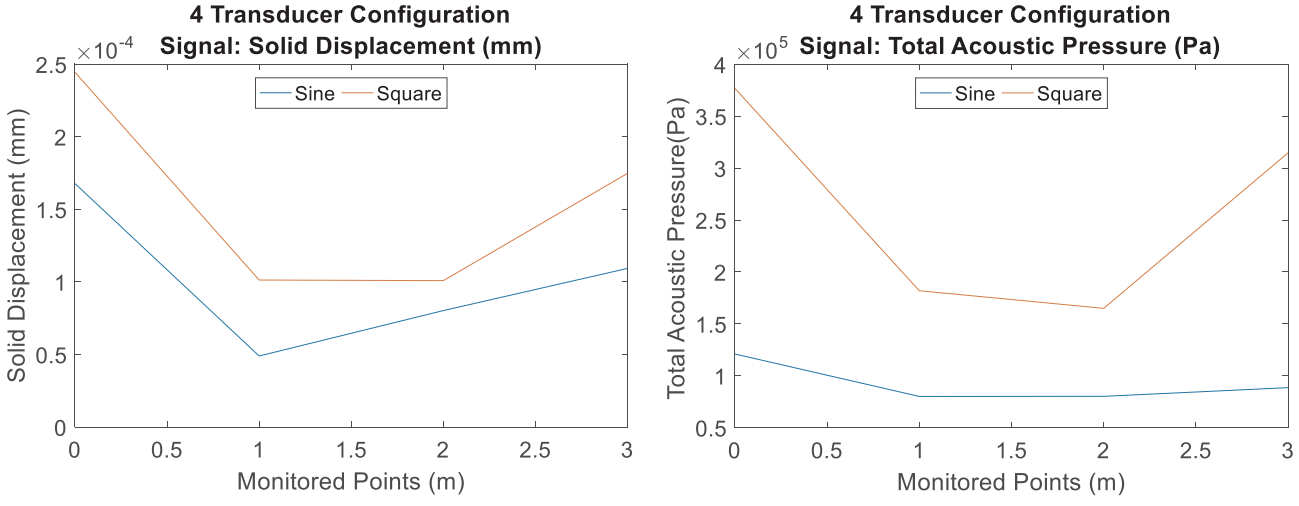

Fig. 15. Maximum solid displacement and pressure acoustic at monitored points for each investigated signal input.

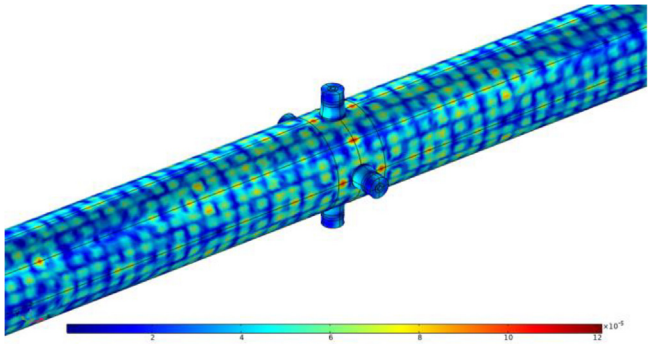

Fig. 16. Pipe displacement of 4-Transducer configuration on 6 in. schedule 40 carbon steel pipe.

increasing effect on the amplitude of both the solid displacement of the pipe and the acoustic pressure of the fluid. The sinusoidal input achieves a lower displacement and acoustic pressure across the structure; however, this can be used for fouling prevention of a clean structure. Ultrasonic prevention will be investigated in further work and also transducer miniaturization to accommodate more transducers around the circumference to achieve more defouling coverage from one transducer location.

Acknowledgments

This investigation was conducted as part of the Innovate UK project HiTClean, grant number 102491. The authors express deep gratitude to Dr. Makis Livadas and Mr. Adrian Waka of Brunel University London for all their efforts and contributions to the project and this work.

References

[1] A.S. Paipetis, T.E. Matikas, D.G. Aggelis, D. Van Hemelrijck, Emerging Technologies in Non-destructive Testing V, CRC Press [Imprint], 2012.
[2] T. Pääkkönen, M. Riihimäki, E. Puhakka, E. Muurinen, C. Simonson, R. Keiski, Crystallization fouling of CaCO3-effect of bulk precipitation on mass deposition on the heat transfer surface, Proceedings of International Conference on Heat Exchanger Fouling and Cleaning VIII, (2009).
[3] B. Bansal, X.D. Chen, Fouling of heat exchangers by dairy fluids - a review, Proceedings of 6th International Conference on Heat Exchanger Fouling and Cleaning, (2005).
[4] X. Guo-qing, D. Z. Han-feng, City Gas Pipeline Burst Analysis Based on MapXtreme, 19. 2014, pp. 9687–9696.
[5] H.-C. Flemming, Reverse osmosis membrane biofouling, Exp. Therm Fluid Sci. 14 (4) (1997) 382–391.
[6] H. Maddah, A. Chogle, Biofouling in reverse osmosis: phenomena, monitoring, controlling and remediation, Appl. Water Science (2016) 1–15.
[7] M.O. Lamminen, Ultrasonic Cleaning of Latex Particle Fouled Membranes, PhD Thesis Ohio State University, USA, 2004.
[8] H. Lais, P.S. Lowe, T.-H. Gan, L.C. Wrobel, Numerical modelling of acoustic pressure fields to optimize the ultrasonic cleaning technique for cylinders, Ultrason. Sonochem. 45 (2018) 7–16.
[9] T.G. Leighton, The acoustic bubble: oceanic bubble acoustics and ultrasonic cleaning, Proc. Meetings Acoustics 24 (1) (2015) 070006.
[10] C. Peng, S. Tian, G. Li, M.C. Sukop, Single-component multiphase lattice Boltzmann simulation of free bubble and crevice heterogeneous cavitation nucleation, Phys. Rev. E 98 (2) (2018) 023305.
[11] C.E. Brennen, Cavitation and Bubble Dynamics, Cambridge University Press, 2013.
[12] S. Muthukumaran, K. Yang, A. Seuren, S. Kentish, M. Ashokkumar, G.W. Stevens, F. Grieser, The use of ultrasonic cleaning for ultrafiltration membranes in the dairy industry, Sep. Purif. Technol. 39 (1) (2004) 99–107.
[13] M.O. Lamminen, H.W. Walker, L.K. Weavers, Mechanisms and factors influencing the ultrasonic cleaning of particle-fouled ceramic membranes, J. Membr. Sci. 237 (1) (2004) 213–223.
[14] H. Lais, P.S. Lowe, J. Kanfoud, T.-H. Gan, Application of high power ultrasonics for fouling removal in submerged structures, IEEE/MTS OCEANS 17 Conference Aberdeen, (2017).
[15] P.S. Lowe, R.M. Sanderson, N.V. Boulgouris, A.G. Haig, W. Balachandran, Inspection of cylindrical structures using the first longitudinal guided wave mode in isolation for higher flaw sensitivity, IEEE Sens. J. 16 (3) (2016) 706–714.
[16] P. Lowe, R. Sanderson, N. Boulgouris, T. Gan, Hybrid active focusing with adaptive dispersion for higher defect sensitivity in guided wave inspection of cylindrical structures, Nondestr. Test. Eval. 31 (3) (2016) 219–234.
[17] G. Mazue, R. Viennet, J.-Y. Hihn, L. Carpentier, P. Devidal, I. Albaïna, Large-scale ultrasonic cleaning system: design of a multi-transducer device for boat cleaning (20kHz), Ultrason. Sonochem. 18 (4) (2011) 895–900.
[18] M.O. Lamminen, H.W. Walker, L.K. Weavers, Effect of fouling conditions and cake layer structure on the ultrasonic cleaning of ceramic membranes, Sep. Sci. Technol. 41 (16) (2006) 3569–3584.
[19] M. Cai, S. Zhao, H. Liang, Mechanisms for the enhancement of ultrafiltration and membrane cleaning by different ultrasonic frequencies, Desalination 263 (1) (2010) 133–138.
[20] S. Muthukumaran, S.E. Kentish, M. Ashokkumar, G.W. Stevens, Mechanisms for the ultrasonic enhancement of dairy whey ultrafiltration, J. Membr. Sci. 258 (1–2) (2005) 106–114.
[21] D.D. Nguyen, H.H. Ngo, Y.S. Yoon, S.W. Chang, H.H. Bui, A new approach involving a multi transducer ultrasonic system for cleaning turbine engines' oil filters under practical conditions, Ultrasonics 71 (2016) 256–263.
[22] Y. Chang, J.H. Bae, H.-C. Yi, Ultrasonic cleaning of used plastic parts for remanufacturing of multifunctional digital copier, Int. J. Precis. Eng. Manuf. 14 (6) (2013) 951–956.
[23] A.P. Mairal, A.R. Greenberg, W.B. Krantz, Investigation of membrane fouling and cleaning using ultrasonic time-domain reflectometry, Desalination 130 (1) (2000) 45–60.
[24] E. Ando, Y. Kagawa, Finite element simulation for the design of an ultrasonic cleaning tank, Electron. Commun. Japan 72 (7) (1989) 43–57.
[25] M. Hill, R.J. Wood, Modelling in the design of a flow-through ultrasonic separator, Ultrasonics 38 (1–8) (2000) 662–665.
[26] E. Heikkola, M. Laitinen, Model-based optimization of ultrasonic transducers, Ultrason. Sonochem. 12 (1–2) (2005) 53–57.
[27] I. Tudela, V. Sáez, M.D. Esclapez, M.I. Díez-García, P. Bonete, J. González-García, Simulation of the spatial distribution of the acoustic pressure in sonochemical reactors with numerical methods: a review, Ultrason. Sonochem. 21 (3) (2014) 909–919.
[28] N. Bretz, J. Strobel, M. Kaltenbacher, R. Lerch, Numerical simulation of ultrasonic waves in cavitating fluids with special consideration of ultrasonic cleaning, Ultrasonics Symposium, 2005 IEEE, 2005, pp. 703–706.
[29] J. Jordens, A. Honings, J. Degrève, L. Braeken, T. Van Gerven, Investigation of design parameters in ultrasound reactors with confined channels, Ultrason. Sonochem. 20 (6) (2013) 1345–1352.
[30] R.E. Caflisch, M.J. Miksis, G.C. Papanicolaou, L. Ting, Effective equations for wave propagation in bubbly liquids, J. Fluid Mech. 153 (1985) 259–273.
[31] K.W. Commander, A. Prosperetti, Linear pressure waves in bubbly liquids: comparison between theory and experiments, J. Acoustical Soc. Am. 85 (2) (1989) 732–746.
[32] C. Vanhille, C. Campos-Pozuelo, Numerical simulations of three-dimensional nonlinear acoustic waves in bubbly liquids, Ultrason. Sonochem. 20 (3) (2013) 963–969.
[33] C. Vanhille, A two-dimensional nonlinear model for the generation of stable cavitation bubbles, Ultrason. Sonochem. 31 (2016) 631–636.
[34] D. Fuster, T. Colonius, Modelling bubble clusters in compressible liquids, J. Fluid Mech. 688 (2011) 352–389.
[35] V. Raman, A. Abbas, S.C. Joshi, Mapping local cavitation events in high intensity ultrasound fields, Excerpt from the Proceeding of the COMSOL Users Conference, Bangalore, 2006, pp. 1–6.
[36] V.S. Sutkar, P.R. Gogate, L. Csoka, Theoretical prediction of cavitational activity distribution in sonochemical reactors, Chem. Eng. J. 158 (2) (2010) 290–295.
[37] J. Klima, A. Frias-Ferrer, J. González-García, J. Ludvik, V. Saez, J. Iniesta, Optimisation of 20 kHz sonoreactor geometry on the basis of numerical simulation of local ultrasonic intensity and qualitative comparison with experimental results, Ultrason. Sonochem. 14 (1) (2007) 19–28.
[38] O. Louisnard, J. Gonzalez-Garcia, I. Tudela, J. Klima, V. Saez, Y. Vargas-Hernandez, FEM simulation of a sono-reactor accounting for vibrations of the boundaries, Ultrason. Sonochem. 16 (2) (2009) 250–259.
[39] E. Gonze, Y. Gonthier, P. Boldo, A. Bernis, Standing waves in a high frequency sonoreactor: visualization and effects, Chem. Eng. Sci. 53 (3) (1998) 523–532.
[40] Y. Asakura, T. Nishida, T. Matsuoka, S. Koda, Effects of ultrasonic frequency and liquid height on sonochemical efficiency of large-scale sonochemical reactors, Ultrason. Sonochem. 15 (3) (2008) 244–250.
[41] O. Louisnard, A viable method to predict acoustic streaming in presence of cavitation, Ultrason. Sonochem. 35 (2017) 518–524.
[42] O. Louisnard, A simple model of ultrasound propagation in a cavitating liquid. Part I: theory, nonlinear attenuation and traveling wave generation, Ultrason. Sonochem. 19 (1) (2012) 56–65.
[43] H. Dogan, V. Popov, Numerical simulation of the nonlinear ultrasonic pressure wave propagation in a cavitating bubbly liquid inside a sonochemical reactor, Ultrason. Sonochem. 30 (2016) 87–97.
[44] R. Jamshidi, G. Brenner, Dissipation of ultrasonic wave propagation in bubbly liquids considering the effect of compressibility to the first order of acoustical Mach number, Ultrasonics 53 (4) (2013) 842–848.
[45] I.M.G.de C. Esteban-Infantes, Fundamentals of Pipeline Cleaning with Acoustic Cavitation, PhD Thesis Brunel University London, UK, 2016.
[46] H. Lais, P. Lowe, J. Kanfoud, T.-H. Gan, Advancements in fouling removal using high power ultrasonics for industrial applications, 2017 IEEE International Conference on Industrial and Information Systems (ICIIS), 2017, pp. 1–6.
[47] K. Yasui, T. Kozuka, T. Tuziuti, A. Towata, Y. Iida, J. King, P. Macey, FEM calculation of an acoustic field in a sonochemical reactor, Ultrason. Sonochem. 14 (5) (2007) 605–614.
[48] M. Ashokkumar, Handbook of Ultrasonics and Sonochemistry, Springer, 2016.

[49] H. Lais, P. Lowe, T.-H. Gan, L. Wrobel, J. Kanfoud, Characterization of the use of low frequency ultrasonic guided waves to detect fouling deposition in pipelines, Sensors 18 (7) (2018) 2122.
[50] A.H. Meitzler, Mode coupling occurring in the propagation of elastic pulses in wires, J. Acoustical Soc. Am. 33 (4) (1961) 435–445.
[51] M. Silk, K. Bainton, The propagation in metal tubing of ultrasonic wave modes equivalent to Lamb waves, Ultrasonics 17 (1) (1979) 11–19.
[52] "Resolving time-dependent waves." [Online]. Available: https://www.comsol.com/support/knowledgebase/1118/. [Accessed: 11-Jun-2016].
[53] K. Yasui, Acoustic cavitation, Acoustic Cavitation and Bubble Dynamics, Springer, 2018, pp. 1–35.